www.czasopisma.pan.pl PAN www.journals.pan.pl
ARCHIVES OF ACOUSTICS Vol. 47, No. 2, pp. 241–257 (2022), doi: 10.24425/aoa.2022.141653

Research Paper

Research on Airflow Background Noise Suppression for Aeroacoustic Wind Tunnel Testing

Yuanwen LI[(1)], Min LI[(2),(3)*], Daofang FENG[(2)], Debin YANG[(1)], Long WEI[(4)]

[(1)] *School of Mechanical Engineering, University of Science and Technology Beijing*
Beijing 100083, China

[(2)] *Collaborative Innovation Center of Steel Technology*
University of Science and Technology Beijing
Beijing 100083, China
*Corresponding Author e-mail: limin@ustb.edu.cn

[(3)] *Key Laboratory of Fluid Interaction with Material, Ministry of Education*
University of Science and Technology Beijing
Beijing 100083, China

[(4)] *Science and Technology on Reliability and Environment Engineering Laboratory*
Beijing Institute of Structure and Environment Engineering
Beijing 100076, China

(*received April 16, 2021; accepted April 11, 2022*)

The microphone data collected in aeroacoustic wind tunnel test contains not only desired aeroacoustic signal but also background noise generated by the jet or the valve of the wind tunnel, so the desired aeroacoustic characteristics is difficult to be highlighted due to the low Signal-to-Noise Ratio (SNR). Classical cross spectral matrix removal can only reduce the microphone self-noise, but its effect is limited for jet noise. Therefore, an Airflow Background Noise Suppression method based on the Ensemble Empirical Mode Decomposition (ABNS-EEMD) is proposed to eliminate the influence of background noise on aeroacoustic field reconstruction. The new method uses EEMD to adaptively separate the background noise in microphone data, which has good practicability for increasing SNR of aeroacoustic signal. A localization experiment was conducted by using two loudspeakers in wind tunnel with 80 m/s velocity. Results show that proposed method can filter out the background noise more effectively and improve the SNR of the loudspeakers signal compared with spectral subtraction and cepstrum methods. Moreover, the aeroacoustic field produced by a NACA EPPLER 862 STRUT airfoil model was also measured and reconstructed. Delay-and-sum beamforming maps of aeroacoustic source were displayed after the background noise was suppressed, which further demonstrates the proposed method's advantage.

Keywords: aeroacoustic measurement; acoustic source localization; EEMD; background noise suppression; wind tunnel test.

1. Introduction

In the past, the research on aircraft noise was mainly focused on engine jet noise, and much work was achieved to reduce the engine noise (SNAKOWSKA *et al.*, 2008; LEE *et al.*, 2018; HUMPHREY *et al.*, 2016). With the development of research, airframe noise generated by the interaction between the fuselage structure and the airflow has attracted more attention (LI *et al.*, 2013; TAO *et al.*, 2016). The airframe noise mainly includes the aeroacoustic sources generated by the lift device, landing gear, wing and tail wings, etc. (TAO *et al.*, 2016; Huang, 2011). To obtain the characteristics of aeroacoustic sources generated by different structures, a large amount of data needs to be accumulated through experiments. The cost of flight test is much

greater than ground measurement, and usually, less data is obtained in flight test. Therefore, the research on aeroacoustic source was mostly focused on different scaled models to carry out the measurements in the acoustic wind tunnel (Mimani *et al.*, 2018; Pan *et al.*, 2019).

The aircraft structure model is placed inside the airflow, and the microphone array is constructed outside a distance to collect the acoustic pressure during the wind tunnel measurement (Merino-Martínez *et al.*, 2018; Suryadi *et al.*, 2017). The aeroacoustics distribution and radiation can be revealed by processing the pressure signal of microphone array. However, the original measured-data by microphone array contains not only desired acoustic signal generated by the interaction between structure model and airflow, but also the background noise caused by jet flow (Bahr *et al.*, 2011). The background noise source may be distributed near the nozzle or diffuser, and the frequency overlap with the desired aeroacoustic signal, resulting in a low Signal-to-Noise Ratio (SNR) of measured-data. Aeroacoustic sources in the beamforming map are disturbed or submerged in the background noise generated by jet flow, which brings great interference to the aeroacoustic source analysis (Bahr *et al.*, 2011; Merino-Martínez *et al.*, 2019). Therefore, the original microphone data, including aeroacoustic signal and background noise, must be pre-processed, so as to highlight the aeroacoustic signal characteristics and provide accurate data support for structural noise-reduction design.

Numerical analysis and measurements of aeroacoustics have shown that there is partial frequency overlap between aeroacoustic signal and background noise (Chong *et al.*, 2013; Vathylakis *et al.*, 2015; Kingan *et al.*, 2009). Traditional methods of background noise removal are often limited by the application environment and highly dependent on human experience, including following three categories: cross-spectral matrix processing, wavenumber processing, and spectral processing. Cross spectral matrix-diagonal removal is widely used to suppress background noise in closed test-section measurement (Hald, Ginn, 2019; Hald, 2017; Bahr *et al.*, 2016; Chiariotti *et al.*, 2019; Porteous *et al.*, 2015). The method works well for microphone self-noise, but its application is limited for the background noise generated by jet flow in open section wind tunnel. Because the jet noise not only exists in the diagonal part, but also exists in the non-diagonal elements. Fischer proposed an improved eigenvalue background noise reduction method which has good effect on microphone self-noise and fan noise, but it works under the assumption that the background noise eigenvectors are orthogonal to the source eigenvectors (Fischer *et al.*, 2020). For the second method related to wavenumber processing, some scholars use the method to suppress the upstream propagating spurious waves by filtering the wavenumber components in different propagation directions (Koop *et al.*, 2008). But the background noise of airflow turbulence in the open section wind tunnel is almost the same as the aeroacoustic signal direction, therefore, the background noise cannot be effectively filtered out.

This paper focuses on the third methods related to spectrum processing.

1) Traditional band-pass filtering can achieve the purpose of signal frequency division (Wei *et al.*, 2017a), but it is difficult to accurately determine the filtering band in the overlapping frequency based on the experience of researchers, so the processing ability of this method for unstable signals is limited (Beck *et al.*, 2005).
2) Spalt *et al.* (2011; 2012) tried to use adaptive noise cancellation method to suppress background noise). However, this kind of method requires a reference signal, and the parameter setting is too complex to be applied in engineering.
3) Spectral subtraction, a method that does not require artificial judgement, is widely used to suppress background noise in frequency-domain (Bahr *et al.*, 2017; Bin *et al.*, 2020; Blacodon *et al.*, 2014). However, the time-domain signal reconstruction must combine the amplitude spectrum obtained by spectral subtraction with the phase of the original signal which is disturbed by the background noise (Blacodon *et al.*, 2014; Boll, 1979). Moreover, the background signals change between measurements will lead to large residual noise levels in the spectral subtraction result (Bahr *et al.*, 2015; Blacodon, 2011).
4) The cepstrum method is also a commonly used denoising method (Boonkla *et al.*, 2017; Fu *et al.*, 2014), which can convert convolution in time-domain into a linear superposition in cepstrum-domain. The mechanism of aeroacoustics is too complicated to be fully expressed by convolution, which limits the effectiveness of cepstrum method to suppress the background noise. Conclusively, there is urgency for studying an effective method that does not depend on the environment and human experience to suppress the background noise generated by jet flow.

Empirical Mode Decomposition (EMD) is also a kind of spectrum processing method, has been widely studied and applied in recent years (Huang *et al.*, 1998; Yang *et al.*, 2016), which can adaptively decompose the signal into different Intrinsic Mode Function (IMF). However, EMD has the problem of mode mixing when the signal is non-stationary. Wu proposed an Ensemble Empirical Mode Decomposition (EEMD) method (Wu *et al.*, 2009), which greatly improves the analysis ability of non-stationary signals through white

noise addition technology. Therefore, the EEMD has been successfully applied in fault diagnosis (Žvokelj *et al.*, 2016), condition monitoring (Liu *et al.*, 2016), and biological signal processing (Taebi *et al.*, 2017). In this paper, EEMD was used to decompose the original microphone data including desired aeroacoustic signal and background noise. The key is that several IMFs representing different characteristic frequencies were obtained to suppress the background noise. Based on the above principles, an Airflow Background Noise Suppression method based on the EEMD (ABNS-EEMD) was proposed to adaptively decrease the interference of airflow in aeroacoustic localization without any prior parameter. In order to verify the effectiveness of the proposed method for background noise suppression, the loudspeaker signals and airfoil model aeroacoustic signals were tested in an open section wind tunnel respectively. Traditional methods are compared with the proposed method to highlight the method's advantages.

The rest of this paper is presented as follows. The principle of the proposed method was introduced in Sec. 2. Then, an experiment that localizes two loudspeakers was carried out under the airflow environment in Sec. 3, and different methods' effects on background noise suppression was discussed in detail. In Sec. 4, aeroacoustic signal of the NACA EPPLER 862 STRUT-airfoil model was measured and localized with the flow speed of 80 m/s. Finally, the study conclusion was provided in Sec. 5.

2. Airflow background noise suppression method based on EEMD

2.1. Theory of EEMD algorithm for processing microphone array signals

Suppose the time-domain signal received by a microphone in the array is $y_m(t)$, where $m = 1, 2, ..., M$ and M is the number of microphones.

Set J groups of white noise $n_j(t)$ with zero mean and constant standard deviation, where $j = 1, 2, ..., J$. In subsequent calculations, an ensemble member of 50 is used, and the added white noise in each ensemble member has a standard deviation of 0.1. The white noise is uncorrelated with each other. J group of the superimposed signal will be obtained after adding different white noise $n_j(t)$ respectively to original microphone *sound* pressure signal $y_m(t)$, and the superimposed signal $y_{m,j}(t)$ can be expressed as:

$$y_{m,j}(t) = y_m(t) + n_j(t). \tag{1}$$

Decompose $y_{m,j}(t)$ by EEMD method and the starting point is the identification of all local maxima and minima of $y_{m,j}(t)$. Then, all local maxima are connected by a cubic spline curve that serves as the upper envelope $h^+_{m,j}(t)$; similarly, all local minima are connected by a spline curve that acts as the lower envelope $h^-_{m,j}(t)$. The mean of the two envelopes is denoted by $h_{m,j}(t)$:

$$h_{m,j}(t) = \frac{h^+_{m,j}(t) + h^-_{m,j}(t)}{2}. \tag{2}$$

The first proto-IMF $c_{m,j,1}(t)$ can be obtained by subtracting $h_{m,j}(t)$ from the signal $y_{m,j}(t)$:

$$c_{m,j,1}(t) = y_{m,j}(t) - h_{m,j}(t). \tag{3}$$

Then, determine whether $c_{m,j,1}(t)$ satisfies the IMF condition:

1) The numbers of extrema and zero-crossings must either be equal or differ at most by one.
2) At any data location, the mean value of the envelope defined by the local maxima and the envelope defined by the local minima is zero.

If $c_{m,j,1}(t)$ satisfies all above criteria, $c_{m,j,1}(t)$ is regarded as the first IMF of signal $y_{m,j}(t)$, and expressed as $\mathrm{IMF}_{m,j,1}(t)$. If $c_{m,j,1}(t)$ does not satisfy all above criteria, $y_{m,j}(t)$ is replaced by $c_{m,j,1}(t)$ as the input signal to be processed, and the operations of formula (2) and (3) are repeated until the obtained $c_{m,j,1}(t)$ meets the two stopping criteria.

The first component $\mathrm{IMF}_{m,j,1}(t)$ obtained previously is subtracted from the initial signal $y_{m,j}(t)$, and the residual $r_{m,j,1}(t)$ can be obtained:

$$r_{m,j,1}(t) = y_{m,j}(t) - \mathrm{IMF}_{m,j,1}. \tag{4}$$

Using the residual $r_{m,j,1}(t)$ as the input signal and repeating steps (2)–(4), we can obtain the 2nd to n-th IMF in sequence, denoted as $\mathrm{IMF}_{m,j,2}(t)$, $\mathrm{IMF}_{m,j,3}(t), ..., \mathrm{IMF}_{m,j,n}(t)$, respectively. The final residual term $r_{m,j,n}(t)$ of the original signal can be expressed as:

$$r_{m,j,n}(t) = r_{m,j,n-1}(t) - \mathrm{IMF}_{m,j,n}. \tag{5}$$

The entire procedure is terminated when residue $r_{m,j,n}(t)$ is a constant, a monotonic slope, or a function with only one extremum. Thus, the original signal $y_{m,j}(t)$ can be expressed as the sum of several IMF and a residual term:

$$y_{m,j}(t) = \sum_{i=1}^{n} \mathrm{IMF}_{m,j,i}(t) + r_{m,j,n}(t). \tag{6}$$

J group set will be obtained after decomposing the m-th collected signal in the M microphones. Average the J group to eliminate the effect of adding white noise on the original signal to obtain i-th IMF of the m-th microphone signal:

$$\mathrm{IMF}_{m,i}(t) = \frac{1}{J} \sum_{j=1}^{J} \mathrm{IMF}_{m,j,i}(t). \tag{7}$$

Each IMF represents the basic characteristics of different frequency bands in the original microphone signal $y_m(t)$, and is arranged in order from high to low frequency, that is, the frequencies of the first IMF is the highest. The original signal $y_m(t)$ can be expressed as:

$$y_m(t) = \sum_{i=1}^{n} \mathrm{IMF}_{m,i}(t) + r_{m,n}(t), \tag{8}$$

where

$$r_{m,n}(t) = \frac{1}{J}\sum_{j=1}^{J} r_{m,j,n}(t).$$

The reason why EEMD can eliminate mode mixing is because there is white noise in each decomposition. The white noise fills all the scale spaces uniformly. Original signal will be projected into the scale space established by the white noise when it is decomposed, eliminating the fitting error of the upper and lower envelopes of the extreme point, effectively decreasing the local interference of the abnormal event on the signal. The decomposition effects are that the added white noise series cancel each other in the final mean of the corresponding IMFs; the mean IMFs stay within the natural dyadic filter windows and thus, significantly reduce the chance of mode mixing and preserve the dyadic property (Wu *et al.*, 2009).

2.2. Background noise suppression

EEMD can adaptively decompose the signal into a series of IMFs with high to low frequencies; however, the selection of IMFs to suppress the background noise is the core of the algorithm.

Assume that no structure is placed in the airflow, and the microphone array is used to collect only the background noise generated by jet. The signal $y_{\mathrm{BG},m}(t)$ collected by the m-th microphone can be expressed as:

$$y_{\mathrm{BG},m}(t) = x_{\mathrm{BG},m}(t)\cdot g_m(t) + e_m(t), \quad m = 1, 2, ..., M, \tag{9}$$

where $y_{\mathrm{BG},m}(t)$ is the background noise collected by the microphone, $x_{\mathrm{BG},m}(t)$ represents the noise generated by the jet flow without structure, $g_m(t)$ denotes the array response function, and $e_m(t)$ shows the random interference noise of the acquisition system.

Using the microphone array to measure the aeroacoustic signal after the structure is placed in the airflow, the signal $y_m(t)$ collected by the m-th microphone also can be expressed as:

$$y_m(t) = x_{\mathrm{BG\text{-}S},m}(t)\cdot g_m(t) + e_m(t), \quad m = 1, 2, ..., M, \tag{10}$$

where $y_m(t)$ is the original microphone data, which contains desired aeroacoustic signal and airflow background noise; $x_{\mathrm{BG\text{-}S},m}(t)$ is the comprehensive pressure generated after putting the structure in airflow, which mainly consists of two parts, one is the background noise $x_{\mathrm{s},m}(t)$ caused by jet flow, and the other is the aeroacoustic signal $s_m(t)$ generated by structure. The aim is to reduce the interference of $x_{\mathrm{s},m}(t)$ from $x_{\mathrm{BG\text{-}S},m}(t)$ and highlight the characteristics of desired signal $s_m(t)$.

First, the decomposition by EEMD is performed sequentially on each original microphone data $y_m(t)$, and n IMFs of each microphone signal are obtained as $\mathrm{IMF}_{m,i}(t)$ $(m = 1, 2, ..., M,\ i = 1, 2, ..., n)$ according to Eqs (1)–(7).

Then, cross-correlation is performed on the component $\mathrm{IMF}_{m,i}(t)$ of the original microphone data $y_m(t)$ and the background noise $y_{\mathrm{BG},m}(t)$. For any value of τ, the correlation coefficient can be calculated by the following equation:

$$R_{m,i} = \max\left\{E\left[y_{\mathrm{BG},m}(t)\mathrm{IMF}_{m,i}(t+\tau)\right]\right\}. \tag{11}$$

For the data collected by any microphone, n correlation coefficients can be obtained, which come from the results of cross correlation calculation between n IMFs and the background noise. Therefore, the average value of n correlation coefficients can be expressed as:

$$\overline{R_m} = \sum_{i=1}^{n} \frac{R_{m,i}}{n}, \quad m = 1, 2, ..., M. \tag{12}$$

The average value $\overline{R_m}$ is taken as a threshold for n IMFs of each original microphone data. A larger correlation coefficient $R_{m,i}$ indicates that the IMF is closer to the background noise and should thus be removed. By contrast, a smaller correlation coefficient $R_{m,i}$ implies that less background noise is contained, suggesting that the IMF mainly originates from the aeroacoustic signal and should thus be reserved. It is assumed that K IMFs with low correlation coefficients are selected, the aeroacoustic signal after the background noise is suppressed can be reconstructed in the time domain (Mariyappa *et al.*, 2014; Chen *et al.*, 2012) as follows:

$$y_m^c = \sum_{k=1}^{K} \mathrm{IMF}_{m,i}^{k}(t), \quad k = 1, 2, ..., K, \tag{13}$$

where y_m^c is the signal of m-th microphone after the background noise is suppressed; $\mathrm{IMF}_{m,i}^{k}(t)$ is the k-th of all IMFs whose correlation coefficient is less than the threshold.

2.3. Summary and flowchart of airflow background noise suppression method

The method proposed in this paper contains two parts. One is to use a microphone array to collect background noise before the structure is placed in the airflow. The second is to keep the airflow and array parameters unchanged, obtaining the original microphone data after putting structure into airflow, and rationally filter the IMF after EEMD decomposition to reconstruct the array signal. The process for this method is briefly explained as follows, and the flowchart is presented in Fig. 1.

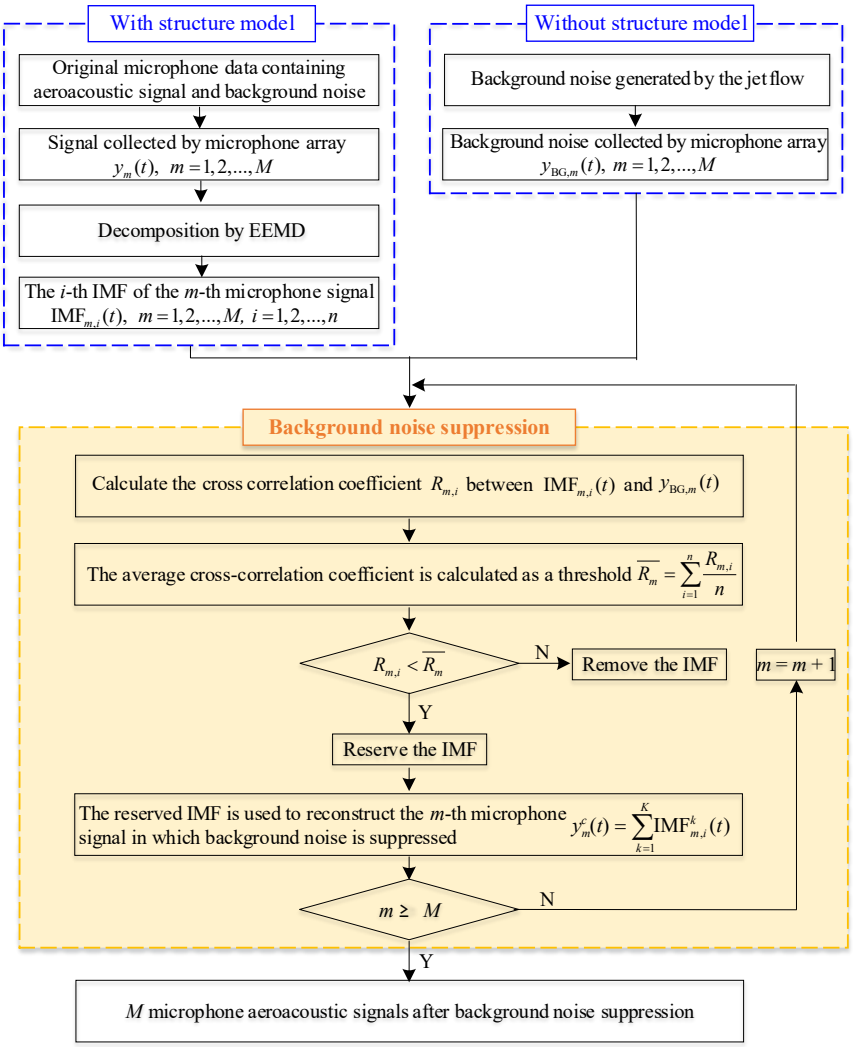

Fig. 1. Flowchart of background noise suppression method.

Step 1: Use an array of M microphones to collect the background noise generated by jet flow without structure and obtain the pressure $y_{\mathrm{BG},m}(t)$, $m = 1, 2, ..., M$.

Step 2: The microphone array is used to collect the original microphone data $y_m(t)$, $m = 1, 2, ..., M$ with structure, and EEMD decomposition is performed to obtain each $\mathrm{IMF}_{m,i}(t)$, $m = 1, 2, ..., M$, $i = 1, 2, ..., n$.

Step 3: The n IMFs of the m-th original microphone data are respectively cross-correlated with the background noise $y_{\mathrm{BG},m}(t)$, and n correlation coefficients $R_{m,i}, i = 1, 2, ..., n$, are obtained.

Step 4: Calculate the average value $\overline{R_m}$ of n correlation coefficients as the threshold.

Step 5: The IMF is reserved in case of $R_{m,i} < \overline{R_m}$.

Step 6: Repeat steps 3 to 5 for all M microphones to obtain the processed array signals which background noise is suppressed. Aeroacoustic source localization can be displayed with the beamforming method.

In summary, the proposed method has the ability of adaptive signal decomposition, which can effectively remove the background noise generated by jet flow and improve the SNR of aeroacoustic signal.

3. Experimental validation and data analysis of background noise suppression

Sound source localization experiment under the airflow interference was carried out for two loudspeakers in the acoustic wind tunnel to verify the proposed method's effectiveness. Different methods were used to suppress the background noise to display the methods' performance.

3.1. Experimental environment and test facilities

The experiment was conducted in an open section wind tunnel with the chamber size of $3.6 \times 3.6 \times 3.2$ m. The top, bottom, and walls of the chamber had sound-absorbent designs. The nozzle had a square cross-sec-

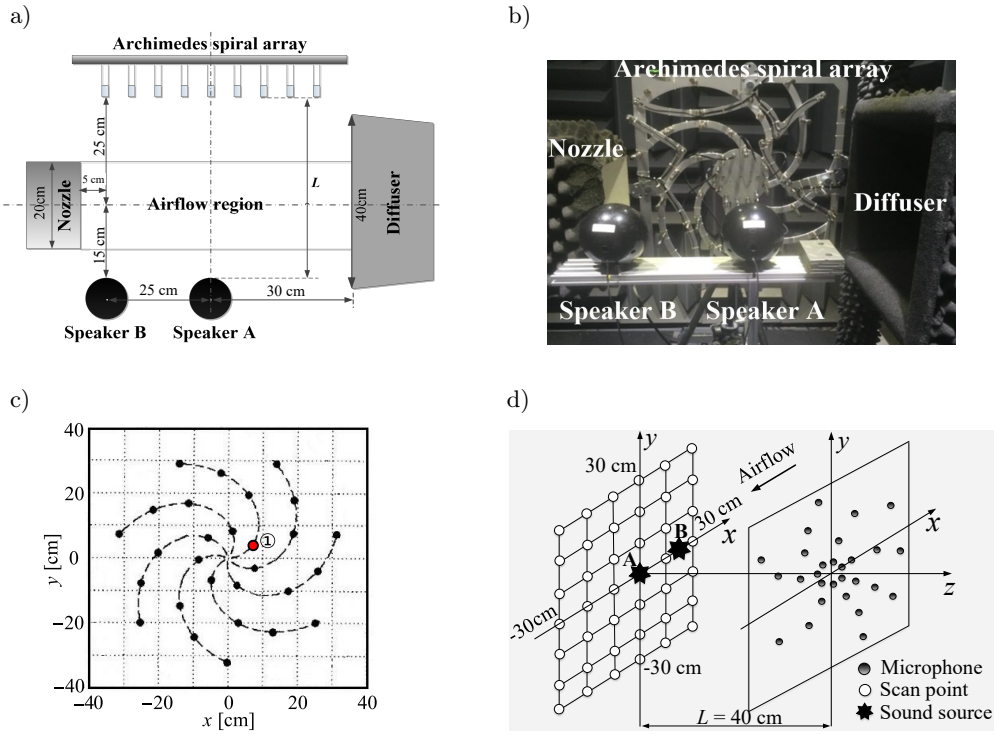

Fig. 2. Experimental environment and layout of facilities: a) schematic diagram of experimental instruments layout, b) experimental instruments, c) Archimedes spiral array, d) position relationship of the array and reconstruction plane in 3D.

tion with a side of 0.2 m, which could generate a stable airflow of 0–80 m/s. The distance between nozzle and diffuser was 0.6 m, which was the test section in the wind tunnel.

Two spherical speakers with a diameter of 9.5 cm were placed as the sound sources on the side of the airflow and were used to generate acoustic signals with different frequency bandwidth. The velocity of airflow was set to 80 m/s to generate background noise. The two speakers were placed on the same side and 15 cm away from the centerline of the airflow as shown in Fig. 2a and 2b. The distance between the two speakers was set to 25 cm, and speaker B was 5 cm away from the nozzle to ensure that the test was carried out in a stable area of airflow. An Archimedes spiral array with a diameter of 64 cm was placed on the other side at a distance of 25 cm away from the central line of airflow, and the measured distance L from the speaker to the microphone array was 40 cm. The Archimedes spiral array consisted of 28 microphones distributed over 7 Archimedean spiral arms, and each arm was equipped with 4 microphones as shown in Fig. 2c. All microphones on the array were BSWA MPA-201 pre-polarized free field microphone. The reconstructed plane measured 60×60 cm and contained 60×60 reconstructed points. The NI-PXIe data acquisition system was used to achieve signal collection with a sampling frequency of 44100 Hz, and 3000 points were sampled.

3.2. Signal processing and spectrum analysis

The limited test space in the acoustic wind tunnel directly affects the size of microphone array and its installation position. According to the experimental setup of Subsec. 3.1, the diameter D of the array was 64 cm, the measured distance L was 40 cm, and the distance between the two sources, the spatial resolution, was $\Delta l = 25$ cm. Generally, the spatial resolution of sound source localization could be calculated by the following formula (Zhang *et al.*, 2019; Luesutthiviboon *et al.* 2019):

$$\Delta l \approx 1.22 \frac{L \cdot c}{D \cdot f}. \tag{14}$$

The Eq. (14) meant that two sources with a distance less than Δl could not be resolved. From Eq. (14), we also knew that in order to accurately identify the two source locations with a distance of 25 cm, the frequency f must be higher than 1000 Hz when the parameters c, L, and D were fixed values. Meanwhile, aeroacoustics sources of aircraft structures are often distributed as multiple broadband noise sources, some broadband noise sources overlap in frequency, while others are distributed in completely different frequency bands (Pagani *et al.*, 2018; Qiao *et al.*, 2016). Therefore, three group signals with different frequency ranges were set in the experiment to verify the proposed method's effectiveness, and the results of each

group are shown in the overall frequency range covering the frequency bands of both loudspeakers:

1) The background noise often covered more than 1000 Hz (Liu *et al.*, 2017; Di Marco *et al.*, 2019), and the aeroacoustic signal was mainly distributed above 1000 Hz with lower energy so that the aeroacoustic signal was seriously interfered by the background noise near 1000 Hz. Therefore, frequency of speaker A was set to 1000–1500 Hz, and speaker B was set to 1500–2000 Hz. In addition, the amplitude of background noise in acoustic wind tunnel was above 0.1 Pa near 1000 Hz, while the amplitude of loudspeakers was less than 0.2 Pa, so the signal was strongly influenced by the background noise.
2) The frequency of speaker A was 1000–3000 Hz, and the speaker B was 2000–4000 Hz. Within this frequency range, background noise had a certain interference with the speaker signal.
3) The frequency of speaker A was 4000–7000 Hz, and speaker B was 5000–8000 Hz. The speaker signal in this frequency range was less disturbed by background noise.

First, the microphone array was used to collect the three groups of speaker signals without airflow; this was used as the reference value after the background noise was suppressed. Then, the wind tunnel started to work, and the airflow was ejected from the nozzle at a steady speed of 80 m/s through debugging. The microphone array collected the background noise after turning off the speaker. Finally, keeping the flow velocity of 80 m/s constant, the speakers sent out the above three groups of signals in sequence, and the original microphone data containing the speaker signal and the background noise were collected. The ABNS-EEMD, spectral subtraction, and cepstrum methods were respectively used to suppress the background noise, and the results were compared with the reference signal collected when there was no airflow:

- spectral subtraction method: The m-th original microphone signal $y_m(t)$ is equally divided into T blocks with overlapping segments, onto which an FFT is applied, and the frequency spectrum of t-th block is written as $P^t(\mathbf{r}_m,\omega)$. The same operation gets the spectrum $P^t_{\mathrm{BG}}(\mathbf{r}_m,\omega)$ of the t-th block of background noise $y_{\mathrm{BG},m}(t)$. Then, the spectrum after suppressing background noise is calculated by averaging all the amplitude difference of T blocks:

$$P(\mathbf{r}_m,\omega) = \frac{1}{\mathrm{T}}\sum_{t=1}^{T}(P^t(\mathbf{r}_m,\omega) - P^t_{\mathrm{BG}}(\mathbf{r}_m,\omega)).$$

- cepstrum method: After obtaining the frequency spectrum $P^t(\mathbf{r}_m,\omega)$ and $P^t_{\mathrm{BG}}(\mathbf{r}_m,\omega)$, they are converted to the cepstrums. The de-noised cepstrum is estimated by subtracting the background noise cepstrum from the original microphone signal cepstrum. And the final cepstrum after suppressing background noise is calculated by averaging all de-noised cepstrums of T block:

$$C(\mathbf{r}_m,\tau) = \frac{1}{\mathrm{T}}\sum_{t=1}^{T}\left[\mathrm{FFT}^{-1}(\log P^t(\mathbf{r}_m,\omega)) - \mathrm{FFT}^{-1}(\log P^t_{\mathrm{BG}}(\mathbf{r}_m,\omega))\right].$$

The frequency spectrum can be recovered by FFT transformation of the cepstrum.

The signal spectrum after the background noise was suppressed by different methods were shown in Fig. 3. To be sure all the results in Fig. 3 were selected from the microphone signal of first channel (shown in Fig. 2c) for display, and the signals of other channels were also the same analysis process.

The first row in Fig. 3 corresponds to the spectrum of speaker signal without airflow interference, and this row is used as a reference signal.

The second row is the spectrum of original microphone data containing the background noise and the speaker signal. It can be seen that the original data collected by the microphone array under the background noise influence had a significant difference with the speaker signal without airflow environment; the energy of original microphone data was mainly distributed in the frequency range below 500 Hz. The characteristics of speaker signal above 1000 Hz were difficult to be highlighted due to airflow interference and were seriously submerged in the background noise.

The third row is the result obtained by spectral subtraction. To some extent, spectral subtraction could suppress the low-frequency background noise, but even so, the energy of background noise was still dominant, and the characteristics of speaker signal were difficult to effectively highlight.

The fourth row is the spectrum after suppressing the background noise by cepstrum method. Compared with spectral subtraction method, the cepstrum method could more effectively suppress the background noise and highlight the characteristics of speaker signal; but the signal processed by the cepstrum method still had background noise components below 500 Hz, which made the SNR of speaker signal still unsatisfactory.

The fifth row is the result after suppressing the background noise by the ABNS-EEMD method. It can be seen that the new method had a positive effect in different frequency ranges for background noise suppression and had more obvious advantages than other methods in the range of 1000–2000 Hz where there was more overlap in the spectrum of the background noise and the speaker signal.

To explicitly quantify the quality of background noise suppression, correlation coefficients were calculated to evaluate the similarity between the spectrum

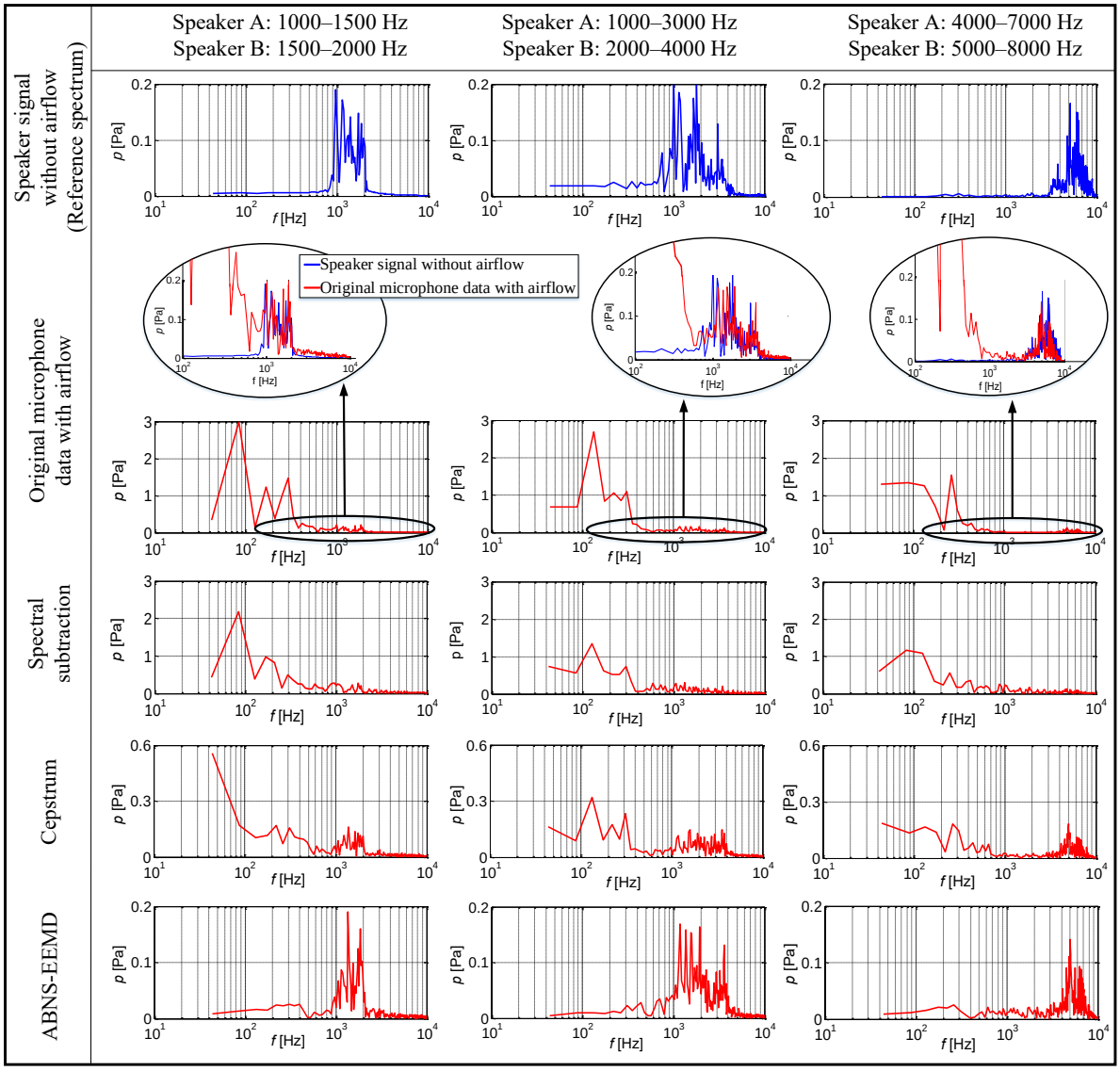

Fig. 3. Spectrum analysis after background noise suppression.

of suppressed signal and the spectrum of reference signal without airflow.

Table 1 shows that the signals obtained by spectral subtraction and cepstrum method have low correlation with the reference signal without airflow. However, the spectrum obtained by ABNS-EEMD method had a positive similarity with the reference spectrum in all frequencies, and the proposed method's advantages was more prominent in low frequency. In order to explain the reason why the ABNS-EEMD method could effectively suppress the background noise, the group (2) data in Fig. 3 was used for analysis, and the results were shown in Fig. 4.

Table 1. Correlation coefficient of the spectrum.

Frequency [Hz]	Speaker A	1000–1500	1000–3000	4000–7000
	Speaker B	1500–2000	2000–4000	5000–8000
Original microphone data		0.346	0.353	0.286
Spectral subtraction		0.392	0.411	0.333
Cepstrum		0.456	0.552	0.601
ABNS–EEMD		0.770	0.768	0.731

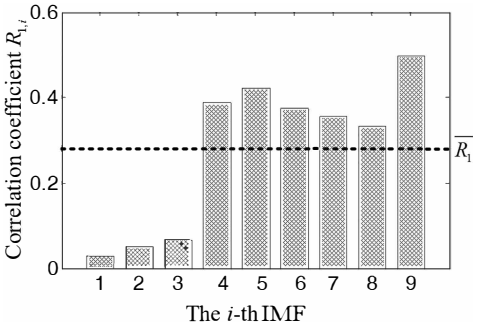

Fig. 4. Correlation coefficient of each IMF obtained by the first channel data.

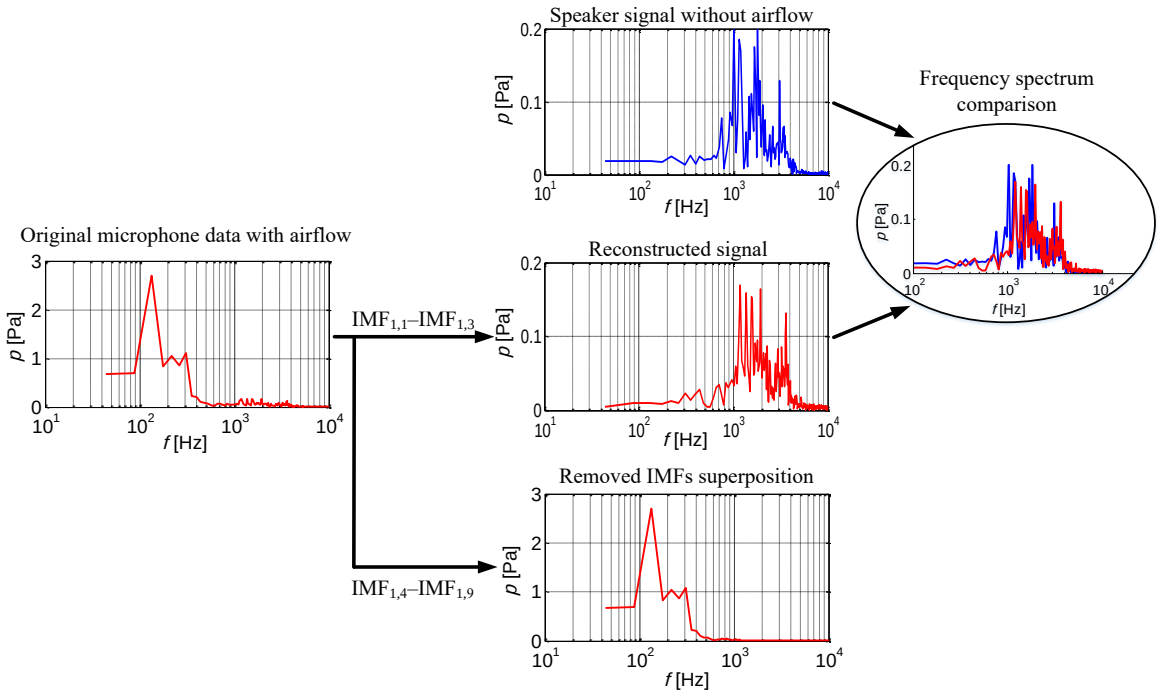

Fig. 5. Signal analysis of the first channel microphone after processed by ABNS-EEMD method.

We have know that after the signal is decomposed by EEMD, a series of sorted IMFs can be obtained, which represent the signal components in the different frequency bands from high frequency to low frequency. The difference characteristics between the signal and the background noise made each IMF have a different correlation coefficient with background noise. The IMF containing the background noise could be accurately identified through the correlation calculation of Eq. (11). Figure 4 shows that the correlation coefficients of the six IMFs with serial numbers 4 to 9 are higher than the threshold, indicating that these six IMFs are very similar to the background noise and should be filtered. IMFs with serial numbers 1 to 3 had very small correlation coefficients with background noise, denoting that these three IMFs mainly contained signal components and should be reserved. The speaker signal should be reconstructed according to formula (13) as shown in Fig. 5.

As can be seen in Fig. 5, the reconstructed signal based on $IMF_{1,1}$–$IMF_{1,3}$ had a high consistency with the speaker signal collected without airflow, which indicated that the reconstructed signal based on $IMF_{1,1}$–$IMF_{1,3}$ could effectively suppress the background noise and retain the frequency characteristics of speaker signal. The correlation of spectrum between reconstructed signal and speaker signal without airflow can be found in Table 1, which is 0.768. Instead, the superposition of removed components based on $IMF_{1,4}$–$IMF_{1,9}$ mainly retained the background noise, so it was similar to the original microphone data collected under the airflow environment. EEMD could adaptively decompose the signal into a finite number of IMFs, which represented the local signals at different scales, so as to separate the airflow background noise from the original microphone data.

3.3. Analysis of the sound source localization results

Conventional delay-and-sum beamforming was used to locate the sound source before and after background noise was suppressed to further analyze the background noise suppression effect. The processed 28 channels array signals were applied, and the localization results of the three group signals are shown in Fig. 6.

The direction of airflow in the beamforming maps of Fig. 6 is from right to left. Two circles in each map represent the actual positions of the loudspeakers with speaker A on the left and speaker B on the right. From Fig. 6, we ascertained the following information.

In the first row, the positions of two sound sources could be better identified for signals with different frequencies when there was no airflow interference.

In the second row, the reconstructed source location seriously deviated from the actual source position due to the influence of high-intensity background noise. The airflow turbulence along the axis in the downstream direction was continuously increasing, causing the turbulence noise sources to be mainly distributed on the left side toward the diffuser. The strong background noise on the left completely buried the speaker location, and the hotspots at the speaker position could not be observed from the beamforming maps.

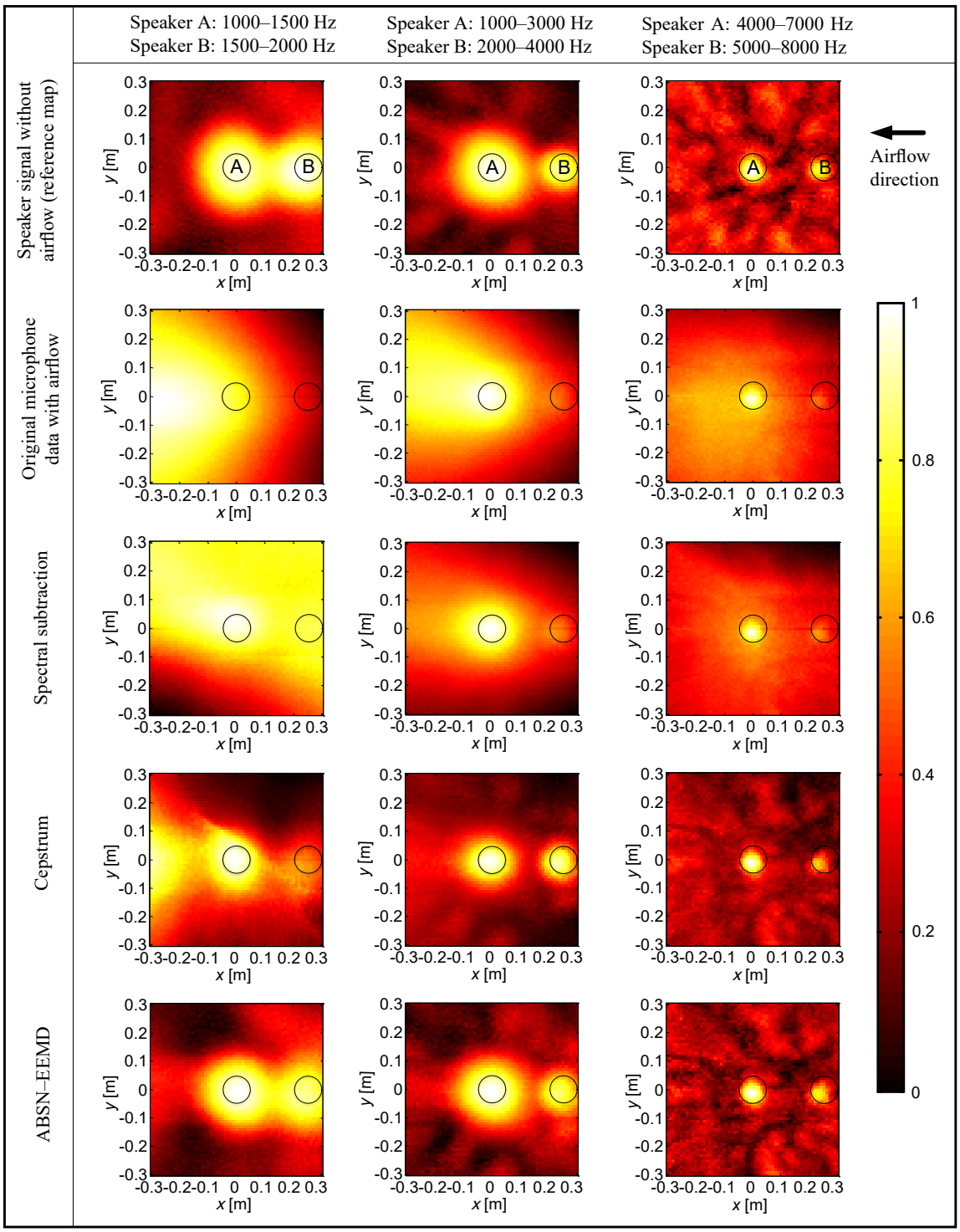

Fig. 6. Normalized beamforming maps of the loudspeakers.

In the third row, Amiet theory was used to modify the propagation path of the acoustic signal to eliminate the airflow influence (Wei *et al.*, 2017a), and the same operation was applied to the results of the fourth and fifth rows. spectral subtraction had a certain suppression effect on the background noise and could display the distribution of two sources at high frequency signals, but it was still unable to accurately identify the source position in the low frequency band (Speaker A: 1000–1500 Hz, Speaker B: 1500–2000 Hz).

In the fourth row, the cepstrum method could effectively be used to identify the source signals at middle and high frequency, but the ability to improve the SNR was limited in the low frequency band (Speaker A:

1000–1500 Hz, Speaker B: 1500–2000 Hz). There were ghosts on the left side of the beamforming maps, which directly affected the localization accuracy.

In the fifth row, the result of ABNS-EEMD method could not only effectively highlight the positions of two speakers but could also be closer to the reconstructed heat area of reference source without airflow. Amplitude of localized source and relative error in three groups of frequency bands were statistically analyzed to quantitatively illustrate the amplitude restoration accuracy. The relative error of the reconstructed source amplitude could be calculated as:

$$\eta = \frac{|W_i - W_0|}{W_0} \times 100\%, \tag{15}$$

where W_i was the amplitude of the reconstructed source after the background noise was suppressed, W_0 was the amplitude of the reconstructed source without airflow. The results are shown in Fig. 7.

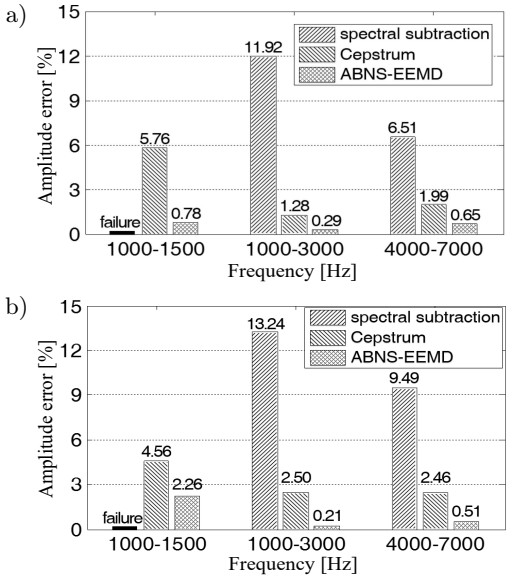

Fig. 7. Quantitative analysis of amplitude error: a) speaker A and b) speaker B.

From Fig. 7 we ascertained the following conclusions:

1) Spectral subtraction was difficult to effectively suppress the background noise, which caused a large error in the source amplitude reconstruction; so, spectrum subtraction could not be used to obtain the amplitude information due to the failure localization in the low frequency band (Speaker A: 1000–1500 Hz, Speaker B: 1500–2000 Hz).
2) Cepstrum method could be used to reconstruct the amplitude information at different frequencies, and the error of the reconstructed amplitude of sound source was lower than that of spectral subtraction.
3) Among the three methods, the reconstruction error of ABNS-EEMD method was the lowest in all of the methods. The proposed method was less than 2.26% at all frequencies, indicating that the method not only had the advantage in sound source localization, but also had the advantage in accurately reconstructing the source amplitude.
4) The reconstructed amplitude error decreased with frequency increasing for all methods. This was because the high frequency signal contained less background noise, and the background noise was mainly distributed at low frequencies, which had a greater impact on the source localization at low frequency.

4. Measurement and analysis of the aeroacoustic signal produced by airfoil model

4.1. Parameter setting of the measurement

The measurement environment used for the aeroacoustic signal produced by an airfoil model was the same anechoic wind tunnel described in Sec. 3. The same microphone array was also utilized, and the placement of the microphone array remained unchanged. The airfoil model used was NACA EPPLER 862 STRUT with a chord length of 12 cm, a span of 40 cm, and a thickness of 3.6 cm as shown in Fig. 8a. The airfoil model was set at the central line of airflow with an attack angle of 0°. The distance between the airfoil model center and nozzle is 30 cm, and the distance between the microphone array and the model was 25 cm as shown in Fig. 8b and 8c. The airflow speed analyzed in this study was still set to 80 m/s. Similarly, the conventional delay-and-sum beamforming maps were calculated on a plane which provided 60×60 cm visualized area and contained 60×60 reconstructed points. The signals were recorded with the same NI-PXIe data acquisition system at a sampling frequency of 44.1 kHz, and 3000 points were sampled.

4.2. Result analysis of the aeroacoustic signal of airfoil model

The generation mechanism of airfoil aeroacoustics is related to frequency. The spectrum was obtained by applying the temporal Fourier transform to original microphone data after the airfoil model was placed in the airflow and compared with the background noise spectrum when there was no airfoil model. Spectrum of the microphone data in first channel before and after putting in the airfoil model is shown in Fig. 9.

According to the amplitude changes in spectrum, Fig. 9 can be divided into two parts: zone I and zone II. In zone I, the background noise spectrum was consistent with the original microphone data spectrum, indicating that the components of original microphone data distributed in the frequency band zone I are mainly background noise. In zone II, the energy of original microphone data was higher than

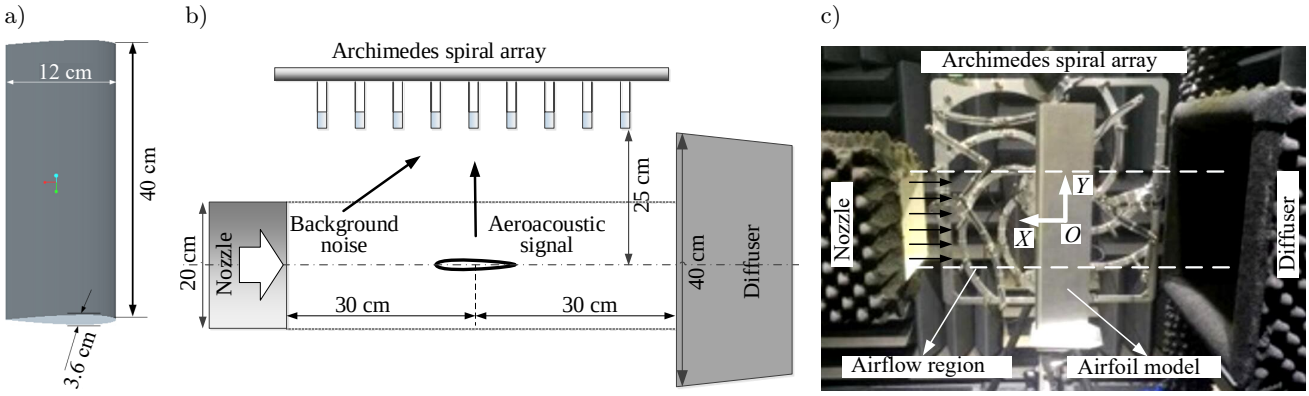

Fig. 8. Layout of the measurement facility for the airfoil model: a) airfoil model, b) schematic diagram of experimental instruments layout, c) the real measurement environment.

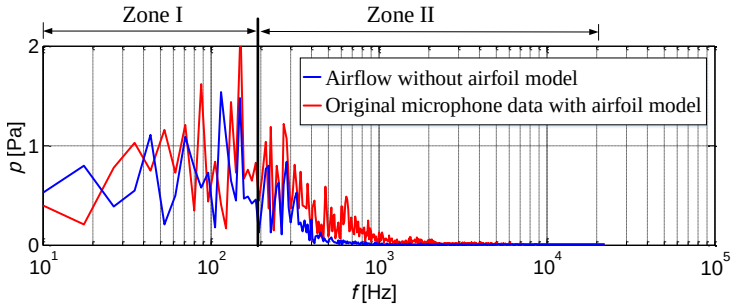

Fig. 9. Frequency spectrum before and after the airfoil model is placed in the airflow.

that of the background noise, meaning that the aeroacoustic signal generated by the airfoil model was mainly distributed in zone II. Simultaneously, there was significant background noise remaining in zone II, which made it difficult for traditional band-pass filtering method to determine the cut-off frequency. Different selection for lower cut-off frequency of the band-pass filter lead to different filtering results, as shown in Fig. 10. It should be noted that with all the results, the researchers used Amiet theory to modify the effect of airflow on sound propagation (Wei *et al.*, 2017b), and normalize all the maps. By using Fig. 10, we ascertained that as the cut-off frequency increased, the background noise contained in the filtered signal decreased, so the reconstructed source location was less interfered by the background noise and gradually approached the airfoil trailing edge (Murayama *at al.*, 2014). From the above analysis, it can be concluded that the selection for cut-off frequency of the band-pass filter would have a great impact on the sound source location. Therefore, we needed to use adaptive methods, such as spectral subtraction, cepstrum,

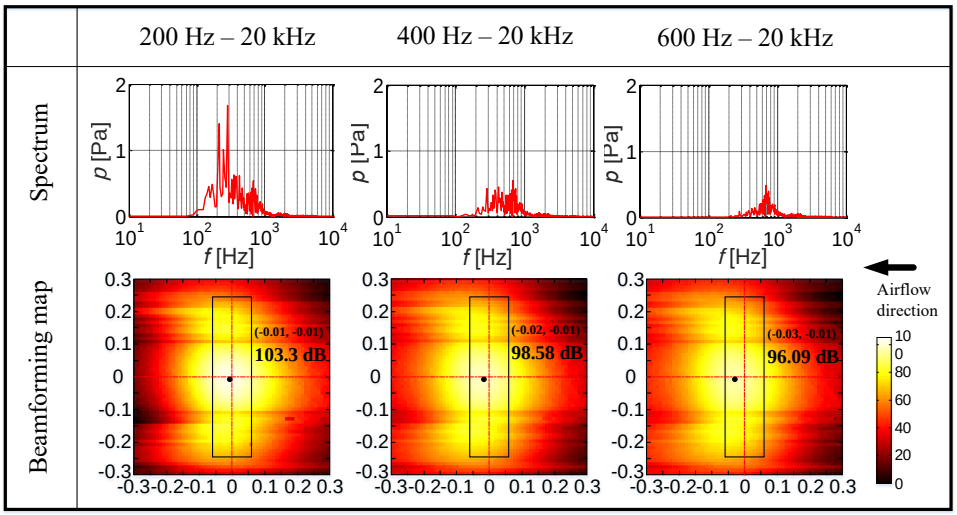

Fig. 10. Normalized results of the band-pass filtering method with different cut-off frequencies.

and ABNS-EEMD, to remove the background noise and improve the location accuracy of sound source.

According to the previous research results, frequency of aeroacoustic signal generated by airfoil model was related to the horizontal coordinate of source location along the airflow axial, mainly including the leading edge noise and trailing edge noise (Chong *et al.*, 2016; Paruchuri *et al.*, 2017). When an airfoil was subjected to an airflow, aeroacoustics was basically generated at both the airfoil leading edge and the trailing edge. Therefore, it could be concluded that zone II included leading edge noise and trailing edge noise as well as part of the background noise. It was necessary to adopt an adaptive method to eliminate the interference of human factors and extract more accurate aeroacoustic signals. The aeroacoustic signal spectrum and delay-and-sum beamforming maps after suppressing the background noise by different adaptive methods are shown in Fig. 11. Similarly, the Amiet theory and normalization are applied in the results.

The first column of Fig. 11 shows the microphone signal spectrum of the first channel before and after the

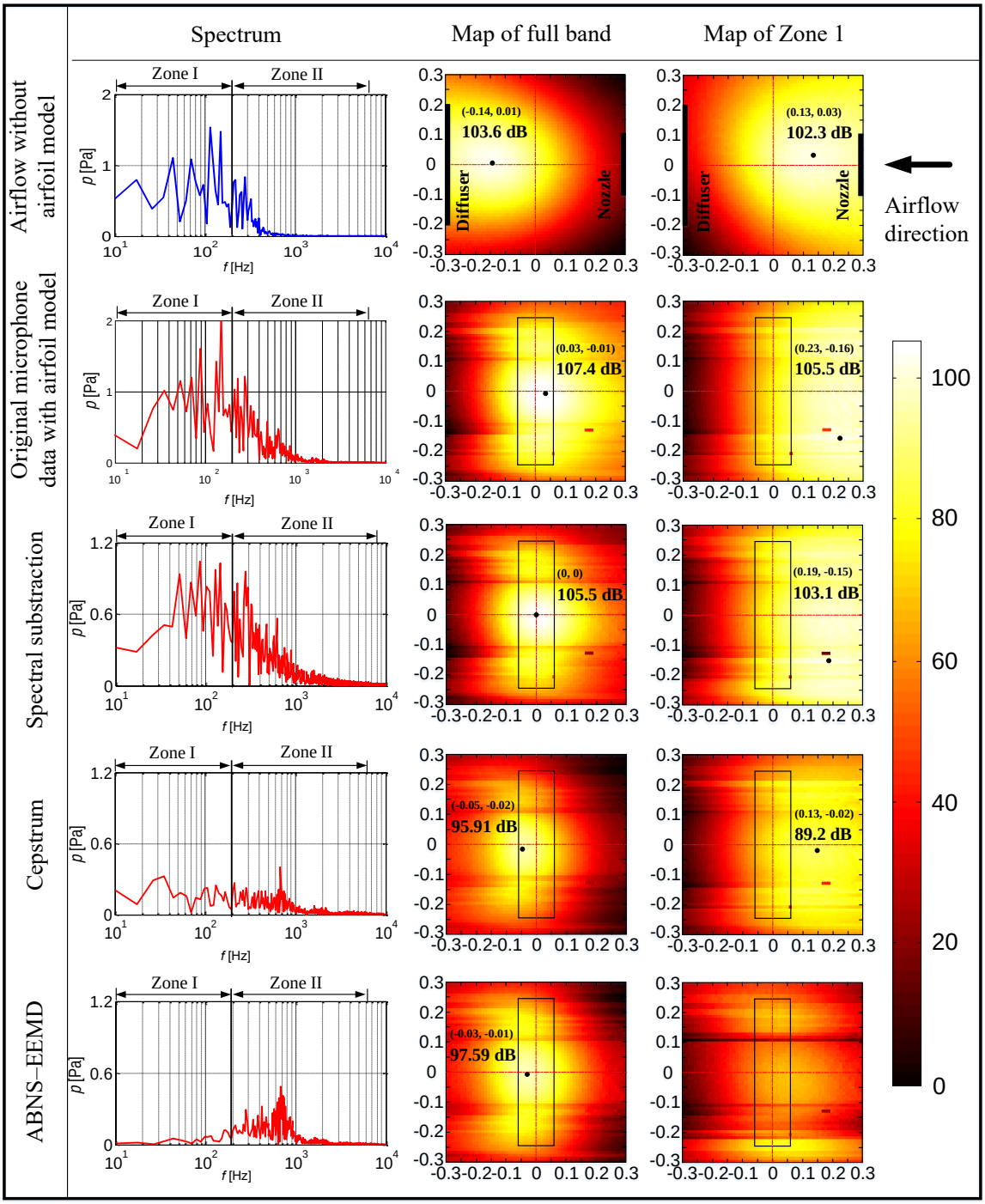

Fig. 11. Spectrum and normalized maps of airfoil model after background noise suppression.

background noise is suppressed by different methods, and the changes in the frequency distribution can be observed intuitively. The second column is the full-band localization maps before and after background noise suppression, which show the different methods' ability to reduce the background noise interference on source localization. The third column is the localization map in zone I. The source is distributed near the nozzle, so it is mainly airflow background noise, which can effectively reflect the proportion of the residual background noise contained in the processed signal.

The first row of Fig. 11 shows the source location of background noise without airfoil model. The background noise is mainly composed of two parts. One is the low-frequency noise of zone I generated by the interaction between airflow and nozzle, which is mainly located near the nozzle. The other is the high-frequency noise which is produced by the airflow turbulence and located at the diffuser downstream of the airflow. The full band map of airflow shows that the reconstructed source is close to the diffuser; this is because the high frequency noise has low amplitude but wide frequency band which makes the total energy of high frequency noise more prominent.

The second row in Fig. 11 is the original microphone data before the background noise is suppressed. The full band result shows that the source is located near the airfoil leading edge, which is the combined effect of background noise and aeroacoustic signal. The localization result of zone I shows that there was a large amount of background noise distributed near the nozzle.

The third row in Fig. 11 shows the result of spectral subtraction method. It can be seen from the spectrum that the energy in zone I had a high amplitude, demonstrating that the aeroacoustic signal was submerged in the background noise and was difficult to be highlighted. By comparing the background noise spectrum of airflow, it can be seen that the result of spectral subtraction method also leaves a large amount of background noise in zone II. The source of band zone I is distributed near the nozzle with extremely high energies, indicating that the spectral subtraction method was difficult to effectively filter out the background noise, which was still dominant in processed signal. The localization result of full band combined the influence of leading edge noise, trailing edge noise, and background noise, thus, the reconstructed source was concentrated in the airfoil model center.

For the cepstrum method in the fourth row of Fig. 11, the interaction mechanism between the airflow and the structure was too complex to describe completely with a convolution relationship, so that the cepstrum method could only be used to filter out part of the background noise. The spectrum of zone I still remained at partial energy, which represented the background noise; meanwhile, energy of zone II in high frequency weakened, resulting in the SNR of the aeroacoustic signal to be relatively low. The energy in beamforming map of zone I was much lower than spectral subtraction, which indicated that cepstrum method had a better suppression effect than spectral subtraction. The reconstructed source in full band was distributed at the trailing edge of the airfoil because the amplitude of the leading-edge noise was reduced, and the residual background noise near to the diffuser also affected the result (Qiao *et al.*, 2018).

The fifth row in Fig.11 display the result of ABNS-EEMD method. A series of IMFs adaptively obtained by the method represent signals in different frequencies and can be used to effectively recognize the difference in the background noise spectrum and aeroacoustic signal compared with the other two methods. Therefore, background noise components can be accurately filtered by different IMFs screening and the SNR of the aeroacoustic signal was improved. The constructed source of full band was located in front of trailing edge due to the combination of leading-edge noise and trailing-edge noise. The results show that ABNS-EEMD had the lowest energy in zone I, effectively suppressing the background noise distributed near the nozzle. In addition, the method also has the ability to filter out the background noise at low frequency and preserve the signal amplitude at high frequency in the zone II, which can obtain a more accurate signal. Although the localization results of the proposed method and cepstrum method were not much different in the full band, ABNS-EEMD contained less background noise, which was more conducive to the aeroacoustic signals analysis.

Based on the three adaptive methods in this paper, the SNR of signal obtained by different methods was calculated to quantify the suppression effect of background noise. The previous analysis showed that major energy of zone I was the background noise, and the aeroacoustic signal was mainly distributed in zone II. Therefore, the SNR of the aeroacoustic signal could be approximately calculated by regarding the total energy in zone II as the useful signal and using the overall energy of zone I as the background noise. SNR could be estimated by the following equation:

$$\mathrm{SNR} = \frac{E_{\text{zone II}}}{E_{\text{zone I}}}, \tag{16}$$

where E is calculated by summing the amplitudes of all frequencies in each zone. The higher of SNR value, the less of the background noise component in the processed signal, and the easier it was to highlight the aeroacoustic signal. The SNR corresponding to each method is shown in Table 2.

In Table 2, the signal processed by ABNS-EEMD method had the highest SNR, indicating that it contained the least background noise, which made the aeroacoustic signal characteristics more prominent

Table 2. The value of SNR of the signal processed by different methods.

Method	Spectral subtraction	Cepstrum	ABNS-EEMD
SNR	3.62	6.00	17.96

than the other methods. The SNR value of ABNS-EEMD method was nearly three times that of the cepstrum method and five times that of the spectral subtraction method.

5. Conclusion

1) This paper proposes an EEMD based method to suppress the background noise generated by jet flow, which can adaptively decompose the original microphone data into different IMFs without setting parameters, so as to identify the difference between the background noise and the aeroacoustic signal. By selecting the IMFs for reconstruction, the background noise can be suppressed, and the SNR of aeroacoustic signal can be improved.
2) A sound source localization experiment was carried out on two speakers at an acoustic wind tunnel with the flow velocity of 80 m/s. Compared with the spectral subtraction and cepstrum methods, the proposed method had the strongest ability to suppress background noise, so that the amplitude error of the localized source corresponding to ABNS-EEMD was less than 2.26%. Moreover, the correlation between the signal extracted by ABNS-EEMD and the reference signal was higher than 0.73, indicating that the new method could be used to remove the background noise interference, which was beneficial to obtain accurate aeroacoustic source location.
3) In the anechoic wind tunnel with a flow speed of 80 m/s, the aeroacoustic source localization of airfoil model was conducted to compare the different methods' effects for suppressing the background noise and improving the SNR in the aeroacoustics measurements. From the perspective of source localization, the localization effect of ABNS-EEMD method is similar to that of cepstrum method, and is better than that of spectral subtraction method. However, the SNR obtained by the ABNS-EEMD method is more than three times that of the other two methods, so the new method can provide accurate aeroacoustic signal for further study of sound field reconstruction.

Acknowledgments

This work is supported by the National Key R&D Program of China (Grant No. 2020YFA0405700) and the National Natural Science Foundation of China (Grant No. 51805036). The authors would also like to thank the editors and reviewers for their valuable suggestions and kind work.

References

1. Bahr C., Li J., Cattafesta L. (2011), Aeroacoustic measurements in open-jet wind tunnels – an evaluation of methods applied to trailing edge noise, *17th AIAA/CEAS Aeroacoustics Conference (32nd AIAA Aeroacoustics Conference)*, Portland, Oregon, USA, Paper No. 2011–2771, doi: 10.2514/6.2011-2771.
2. Bahr C.J., Cattafesta L.N. (2016), Wavenumber–frequency deconvolution of aeroacoustic microphone phased array data of arbitrary coherence, *Journal of Sound and Vibration*, **382**: 13–42, doi: 10.1016/j.jsv.2016.06.044.
3. Bahr C.J., Horne W.C. (2015), Advanced background subtraction applied to aeroacoustic wind tunnel testing, [in:] *21st AIAA/CEAS Aeroacoustics Conference*, p. 3272, doi: 10.2514/ 6.2015-3272.
4. Bahr C.J., Horne W.C. (2017), Subspace-based background subtraction applied to aeroacoustic wind tunnel testing, *International Journal of Aeroacoustics*, **16**(4–5): 299–325, doi: 10.1177/1475472x17718885.
5. Beck T.W. *et al.* (2005), Comparison of Fourier and wavelet transform procedures for examining the mechanomyographic and electromyographic frequency domain responses during fatiguing isokinetic muscle actions of the biceps brachii, *Journal of Electromyography and Kinesiology*, **15**(2): 190–199, doi: 10.1016/j.jelekin.2004.08.007.
6. Bin F., Lei X. (2020), The combination of spectrum subtraction and cross-power spectrum phase method for time delay estimation, *Archives of Acoustics*, **45**(3): 453–458, doi: 10.24425/aoa.2020.134061.
7. Blacodon D. (2011), Array processing for noisy data: Application for open and closed wind tunnels, *AIAA Journal*, **49**(1): 55–66, doi: 10.2514/1.J050006.
8. Blacodon D., Bulté J. (2014), Reverberation cancellation in a closed test section of a wind tunnel using a multi-microphone cesptral method, *Journal of Sound and Vibration*, **333**(9): 2669–2687, doi: 10.1016/j.jsv.2013.12.012.
9. Boll S. (1979), Suppression of acoustic noise in speech using spectral subtraction, *IEEE Transactions on Acoustics, Speech, and Signal Processing*, **27**(2): 113–120, doi: 10.1109/TASSP.1979.1163209.
10. Boonkla S., Unoki M., Wutiwiwatchai C., Makhanov S.S. (2017), F_0 estimation using empirical mode decomposition and complex cepstrum analysis in reverberant environments, *2017 Asia–Pacific Signal and Information Processing Association Annual Summit and Conference (APSIPA ASC)*, Kuala Lumpur, Malaysia, December 12–15, Paper No. 17562827, doi: 10.1109/apsipa.2017.8282165.
11. Chen W., Wang S., Zhang Z., Chuai X. (2012), Noise reduction based on wavelet threshold filtering

and ensemble empirical mode decomposition, *SEG Technical Program Expanded Abstracts*, September 01, Paper No. 4609, doi: 10.1190/segam2012-0567.1.

12. Chiariotti P., Martarelli M., Castellini P. (2019), Acoustic beamforming for noise source localization–Reviews, methodology and applications, *Mechanical Systems and Signal Processing*, **120**: 422–448, doi: 10.1016/j.ymssp.2018.09.019.
13. Chong T.P., Dubois E. (2016), Optimization of the poro-serrated trailing edges for airfoil broadband noise reduction, *The Journal of the Acoustical Society of America*, **140**(2): 1361–1373, doi: 10.1121/1.4961362.
14. Chong T.P., Joseph P.F., Kingan M.J. (2013), An investigation of airfoil tonal noise at different Reynolds numbers and angles of attack, *Applied Acoustics*, **74**(1): 38–48, doi: 10.1016/j.apacoust.2012.05.016.
15. Di Marco A. *et al.* (2019), Airframe noise measurements in a large hard-walled closed-section wind tunnel, *Applied Acoustics*, **146**: 96–107, doi: 10.1016/j.apacoust.2018.11.006.
16. Fischer J., Doolan C. (2020), An improved eigenvalue background noise reduction method for acoustic beamforming, *Mechanical Systems and Signal Processing*, **140**: 106702, doi: 10.1016/j.ymssp.2020.106702.
17. Fu Q., Wei L., Yang D., Li M. (2014), Reflected acoustic wave suppression method based on the cepstrum clip and its application in noise field reconstruction, [in Chinese] *Chinese Journal of Engineering*, **36**(6): 845–854, doi: 10.13374/j.issn1001-053x.2014.06.020.
18. Hald J. (2017), Removal of incoherent noise from an averaged cross-spectral matrix, *The Journal of the Acoustical Society of America*, **142**(2): 846–854, doi: 10.1121/1.4997923.
19. Hald J., Ginn K.B. (2019), Cross-spectral matrix denoising for beamforming in wind tunnels, [in:] *INTER-NOISE and NOISE-CON Congress and Conference Proceedings*, Vol. 259, No. 6, pp. 3516-3527, Madrid, Spain, June 16–19.
20. Huang N.E. *et al.* (1998), The empirical mode decomposition and the Hilbert spectrum for nonlinear and non-stationary time series analysis, *Proceedings of the Royal Society of London. Series A*, **454**(1971): 903–995, doi: 10.1098/rspa.1998.0193.
21. Huang X. (2011), Real-time location of coherent sound sources by the observer-based array algorithm, *Measurement Science and Technology*, **22**(6): 065501, doi: 10.1088/0957-0233/22/6/065501.
22. Humphrey N.J., Edgington-Mitchell D. (2016), The effect of low lobe count chevron nozzles on supersonic jet screech, *International Journal of Aeroacoustics*, **15**(3): 294–311, doi: 10.1177/1475472x16630872.
23. Kingan M.J., Pearse J.R. (2009), Laminar boundary layer instability noise produced by an aerofoil, *Journal of Sound and Vibration*, **322**(4–5): 808–828, doi: 10.1016/j.jsv.2008.11.043.
24. Koop L., Ehrenfried K. (2008), Microphone-array processing for wind-tunnel measurements with strong background noise, *14th AIAA/CEAS Aeroacoustics Conference (29th AIAA Aeroacoustics Conference)*, Vancouver, British Columbia, Canada, May 5–7, Paper No. 2008-2907, doi: 10.2514/6.2008-2907.
25. Lee I., Zhang Y., Lin D. (2018), A model-scale test on noise from single-stream nozzle exhaust geometries in static conditions, *Chinese Journal of Aeronautics*, **31**(12): 2206–2220, doi: 10.1016/j.cja.2018.08.001.
26. Li Y., Wang X., Zhang D. (2013), Control strategies for aircraft airframe noise reduction, *Chinese Journal of Aeronautics*, **26**(2): 249–260, doi: 10.1016/j.cja.2013.02.001.
27. Liu P., Xing Y., Guo H., Li L. (2017), Design and performance of a small-scale aeroacoustic wind tunnel, *Applied Acoustics*, **116**: 65–69, doi: 10.1016/j.apacoust.2016.09.014.
28. Liu W.Y., Tang B.P., Han J.G., Lu X.N., Hu N.N., He Z.Z. (2015), The structure healthy condition monitoring and fault diagnosis methods in wind turbines: A review, *Renewable and Sustainable Energy Reviews*, **44**: 466–472, doi: 10.1016/j.rser.2014.12.005.
29. Luesutthiviboon S., Malgoezar A.M.N., Merino-Martinez R., Snellen M., Sijtsma P., Simons D.G. (2019), Enhanced HR-CLEAN-SC for resolving multiple closely spaced sound sources, *International Journal of Aeroacoustics*, **18**(4–5): 392–413, doi: 10.1177/1475472X19852938.
30. Mariyappa N. *et al.* (2014), Baseline drift removal and denoising of MCG data using EEMD: role of noise amplitude and the thresholding effect, *Medical Engineering & Physics*, **36**(10): 1266–1276, doi: 10.1016/j.medengphy.2014.06.023.
31. Merino-Martínez R. *et al.* (2018), Comparison between analog and digital phased microphone arrays for aeroacoustic measurements, *AIAA/CEAS Aeroacoustics Conference*, Atlanta, Georgia, USA, June. 25–29, Paper No. 2018–2809, doi: 10.2514/6.2018-2809.
32. Merino-Martínez R. *et al.* (2019), A review of acoustic imaging methods using phased microphone arrays, *CEAS Aeronautical Journal*, **10**(1): 197–230, doi: 10.1007/s13272-019-00383-4.
33. Mimani A., Fischer J., Moreau D.J., Doolan C.J. (2018), A comparison of time-reversal and cross-spectral beamforming for localizing experimental rod-airfoil interaction noise sources, *Mechanical Systems and Signal Processing*, **111**: 456–491, doi: 10.1016/j.ymssp.2018.03.029.
34. Murayama M., Nakakita K., Yamamoto K., Ura H., Ito Y., Choudhari M.M. (2014), Experimental study on slat noise from 30p30n three-element high-lift airfoil at JAXA hard-wall lowspeed wind tunnel, *20th AIAA/CEAS Aeroacoustics Conference*, Atlanta, GA, USA, June. 16–20, Paper No. 2014–2080, doi: 10.2514/6.2014-2080.
35. Pagani Jr C.C., Souza D.S., Medeiros M.A. (2016), Slat noise: aeroacoustic beamforming in closed-section wind tunnel with numerical comparison, *AIAA Journal*, **54**(7): 2100–2115, doi: 10.2514/1.J054042.

36. Pan X., Wu H., Jiang W. (2019), Multipole orthogonal beamforming combined with an inverse method for coexisting multipoles with various radiation patterns, *Journal of Sound and Vibration*, **463**: 114979, doi: 10.1016/j.jsv.2019.114979.

37. Paruchuri C. *et al.* (2017), Performance and mechanism of sinusoidal leading edge serrations for the reduction of turbulence-aerofoil interaction noise, *Journal of Fluid Mechanics*, **818**: 435–464, doi: 10.1017/jfm.2017.141.

38. Porteous R., Prime Z., Doolan C.J., Moreau D.J., Valeau V. (2015), Three-dimensional beamforming of dipolar aeroacoustic sources, *Journal of Sound and Vibration*, **355**: 117–134, doi: 10.1016/j.jsv.2015.06.030.

39. Qiao W.Y., Ji L., Tong F., Wang L.F., Chen W.J. (2018), Separation and quantification of airfoil LE- and TE-noise source with microphone array, *7th Berlin Beamforming Conference*, Berlin, Germany, March 5–8, Paper No. BeBeC2018 D-14.

40. Snakowska A., Idczak H. (2008), Prediction of turbofan engine noise considering diffraction at the duct outlet, *Archives of Acoustics*, **33**(4): 129–134.

41. Spalt T., Fuller C., Brooks T., Humphreys W. (2011), A background noise reduction technique using adaptive noise cancellation for microphone arrays, *17th AIAA/CEAS Aeroacoustics Conference (32nd AIAA Aeroacoustics Conference)*, Portland, Oregon, USA, June 05–08, Paper No. 2011-2715, doi: 10.2514/6.2011-2715.

42. Spalt T.B., Fuller C.R., Brooks T.F. (2012), Background noise reduction using adaptive noise cancellation determined by the cross-correlation, *Inter-Noise Conference*, New York, USA, August 19–22.

43. Suryadi A., Martens S., Herr M. (2017), Trailing edge noise reduction technologies for applications in wind energy, *23rd AIAA/CEAS Aeroacoustics Conference*, Denver, Colorado, USA, June 5–9, Paper No. 2017-3534, doi: 10.2514/6.2017-3534.

44. Taebi A., Mansy H.A. (2017), Noise cancellation from vibrocardiographic signals based on the ensemble empirical mode decomposition, *Journal of Applied Biotechnology & Bioengineering*, **2**(2): 00024, doi: 10.15406/jabb.2017.02.00024.

45. Tao J., Sun G. (2016), An artificial neural network approach for aerodynamic performance retention in airframe noise reduction design of a 3D swept wing model, *Chinese Journal of Aeronautics*, **29**(5): 1213–1225, doi: 10.1016/j.cja.2016.08.008.

46. Vathylakis A., Chong T.P., Joseph P.F. (2015), Poro-serrated trailing-edge devices for airfoil self-noise reduction, *AIAA Journal*, **53**(11): 3379–3394, doi: 10.2514/1.j053983.

47. Wei L., Li M., Qin S., Fu Q., Yang D. (2017a), Sound source localization method in an environment with flow based on Amiet–IMACS, *Mechanical Systems and Signal Processing*, **88**: 240–252, doi: 10.1016/j.ymssp.2016.11.011.

48. Wei L., Li M., Yang D., Niu F., Zeng W. (2017b), Reconstruction of sound source signal by analytical passive TR in the environment with airflow, *Journal of Sound and Vibration*, **392**: 77–90, doi: 10.1016/j.jsv.2016.12.040.

49. Wu Z., Huang N.E. (2009), Ensemble empirical mode decomposition: a noise-assisted data analysis method, *Advances in Adaptive Data Analysis*, **1**(01): 1–41, doi: 10.1142/s1793536909000047.

50. Yang D., Li H., Hu Y., Zhao J., Xiao H., Lan Y. (2016), Vibration condition monitoring system for wind turbine bearings based on noise suppression with multi-point data fusion, *Renewable Energy*, **92**, 104–116, doi: 10.1016/j.renene.2016.01.099.

51. Zhang C.Q. *et al.* (2019), Locating and tracking sound sources on a horizontal axis wind turbine using a compact microphone array based on beamforming, *Applied Acoustics*, **146**: 295–309, doi: 10.1016/j.apacoust.2018.10.006.

52. Žvokelj M., Zupan S., Prebil I. (2016), EEMD-based multiscale ICA method for slewing bearing fault detection and diagnosis, *Journal of Sound and Vibration*, **370**: 394–423, doi: 10.1016/j.jsv.2016.01.046.